

⁸⁹Zr-Bevacizumab PET Imaging in Primary Breast Cancer

Sietske B.M. Gaykema¹, Adrienne H. Brouwers², Marjolijn N. Lub-de Hooge^{2,3}, Rick G. Pleijhuis⁴, Hetty Timmer-Bosscha¹, Linda Pot¹, Gooitzen M. van Dam⁴, Sibylle B. van der Meulen⁵, Johan R. de Jong², Joost Bart⁶, Jakob de Vries⁴, Liesbeth Jansen⁴, Elisabeth G.E. de Vries¹, and Carolien P. Schröder¹

¹Department of Medical Oncology, University Medical Center Groningen, Groningen, The Netherlands; ²Department of Nuclear Medicine and Molecular Imaging, University Medical Center Groningen, Groningen, The Netherlands; ³Department of Hospital and Clinical Pharmacy, University Medical Center Groningen, Groningen, The Netherlands; ⁴Department of Surgical Oncology, University Medical Center Groningen, Groningen, The Netherlands; ⁵Department of Radiology, University Medical Center Groningen, Groningen, The Netherlands; and ⁶Department of Pathology, University Medical Center Groningen, Groningen, The Netherlands

Vascular endothelial growth factor (VEGF)-A is overexpressed in most malignant and premalignant breast lesions. VEGF-A can be visualized noninvasively with PET imaging and using the tracer ⁸⁹Zr-labeled bevacizumab. In this clinical feasibility study, we assessed whether VEGF-A in primary breast cancer can be visualized by ⁸⁹Zr-bevacizumab PET. **Methods:** Before surgery, breast cancer patients underwent a PET/CT scan of the breasts and axillary regions 4 d after intravenous administration of 37 MBq of ⁸⁹Zr-bevacizumab per 5 mg. PET images were compared with standard imaging modalities. ⁸⁹Zr-bevacizumab uptake was quantified as the maximum standardized uptake value (SUV_{max}). VEGF-A levels in tumor and normal breast tissues were assessed with enzyme-linked immunosorbent assay. Data are presented as mean ± SD. **Results:** Twenty-five of 26 breast tumors (mean size ± SD, 25.1 ± 19.8 mm; range, 4–80 mm) in 23 patients were visualized. SUV_{max} was higher in tumors (1.85 ± 1.22; range, 0.52–5.64) than in normal breasts (0.59 ± 0.37; range, 0.27–1.69; *P* < 0.001). The only tumor not detected on PET was 10 mm in diameter. Lymph node metastases were present in 10 axillary regions; 4 could be detected with PET (SUV_{max}, 2.66 ± 2.03; range, 1.32–5.68). VEGF-A levels in the 17 assessable tumors were higher than in normal breast tissue in all cases (VEGF-A/mg protein, 184 ± 169 pg vs. 10 ± 21 pg; *P* = 0.001), whereas ⁸⁹Zr-bevacizumab tumor uptake correlated with VEGF-A tumor levels (*r* = 0.49). **Conclusion:** VEGF-A in primary breast cancer can be visualized by means of ⁸⁹Zr-bevacizumab PET.

Key Words: breast cancer; VEGF-A; ⁸⁹Zr-bevacizumab PET; early detection

J Nucl Med 2013; 54:1014–1018

DOI: 10.2967/jnumed.112.117218

Breast cancer is the most common cause of cancer-related deaths among women (1). The application of molecular imaging can visualize and potentially quantifies functional differences between tumor and normal cells. A molecular target of interest in this respect is vascular endothelial growth factor (VEGF)-A. VEGF-A is

involved in the development and maintenance of tumor angiogenesis and is involved early during tumorigenesis. Various studies have reported overexpression of VEGF-A in the breast cancer microenvironment, compared with normal breast tissue (2–5). All VEGF-A splice variants are bound by the clinically used monoclonal antibody bevacizumab. When labeled with the PET isotope ⁸⁹Zr, bevacizumab preserves its VEGF-A-binding properties. Thus, tracer dosages of radiolabeled bevacizumab can be used for tumor-specific, whole-body imaging of VEGF-A. In preclinical studies (6,7) and in a study in renal cell cancer patients (8), we have already shown an excellent tumor-to-background ratio with an optimum at 4 d after tracer injection when using ⁸⁹Zr-bevacizumab. In the present clinical feasibility study, we used ⁸⁹Zr-bevacizumab PET to provide proof of principle on whether VEGF-A imaging can be used for detection of primary breast tumors.

MATERIALS AND METHODS

Patients

Eligible patients had a histologically or cytologically confirmed adenocarcinoma of the breast and were scheduled for mastectomy or lumpectomy. Additional eligibility criteria included a minimum age of 18 y and World Health Organization performance status of no more than 2. In all patients, standard diagnostics consisted of mammography and ultrasonography. When needed to better define tumor extent, MR imaging was also performed. Exclusion criteria included pregnancy or lactation, prior radiotherapy in the involved area, major surgery within 28 d before initiation of the study, clinically significant cardiovascular disease, or prior allergic reactions to immunoglobulins. In premenopausal patients, a pregnancy test was performed to exclude pregnancy.

The study was approved by the Medical Ethics Committee of the University Medical Center of Groningen. This local committee was supervised by the Central Committee on Research Involving Human Subjects, which acts as the competent authority. All patients gave written informed consent. The trial is registered under clinicaltrials.gov number NCT00991978.

⁸⁹Zr-Bevacizumab PET Imaging

Patients received 37 MBq of ⁸⁹Zr-bevacizumab per 5 mg of protein as an intravenous bolus injection 4 d before PET scanning and were observed for allergic reactions for 1 h. The 5-mg dose of bevacizumab was chosen because this was the lowest possible dose that was reproducible during the labeling procedure. The same dose was used in a study with ¹¹¹In-labeled bevacizumab, which visualized all known melanoma lesions (9). ⁸⁹Zr has a decay half-life of 78.4 h, the mean β-energy is 395.5 keV, the positron branching fraction is 22.74%, and the main γ-emissions are 511 keV, 45.5%, and 909 keV, 99.04%.

Received Nov. 26, 2012; revision accepted Jan. 28, 2013.

For correspondence or reprints contact: Carolien P. Schröder, Department of Medical Oncology, University Medical Center Groningen, P.O. Box 30001, 9700 RB Groningen, the Netherlands.

E-mail: C.P.Schröder@umcg.nl

Published online May 7, 2013.

COPYRIGHT © 2013 by the Society of Nuclear Medicine and Molecular Imaging, Inc.

Clinical ^{89}Zr -bevacizumab was produced as follows: reconstituted bevacizumab (Avastin; Roche) was conjugated with tetrafluorophenol-*N*-succinyl-desferal-Fe (VU University Medical Center), purified, and stored at -80°C . Good manufacturing practice-produced ^{89}Zr -oxalate (BV Cyclotron) was used for radiolabeling the conjugate. Quality control was performed to ensure radiochemical purity ($>95\%$), antigen binding, and stability. PET/CT was performed with a Biograph mCT 64-slice PET/CT camera (Siemens). Scanning of both breasts and the axillary regions was performed in 2 bed positions with 5 min of imaging per bed position. In addition, a low-dose CT scan was performed and was used for attenuation and scatter correction. The patient was positioned prone with the breasts hanging. PET data were reconstructed with Siemens iterative reconstruction, involving 3-dimensional ordinary Poisson ordered-subsets expectation maximization without time-of-flight and point-spread-function methods. The settings used for reconstruction were 2 iterations and 8 subsets, a matrix size of 200, and a postprocessing filter of 10 mm, resulting in an effective resolution of 11 mm. For sentinel lymph node detection and SPECT imaging as standard of care, 100 MBq of $^{99\text{m}}\text{Tc}$ -labeled nanocolloid were administered 1 d before surgery. To avoid interference of SPECT imaging, a minimal interval of 3 half-life episodes of ^{89}Zr -bevacizumab (11 d) was considered between the administration of ^{89}Zr -bevacizumab and $^{99\text{m}}\text{Tc}$ -nanocolloid to allow for sufficient ^{89}Zr isotope decay.

^{89}Zr -Bevacizumab PET Analysis

Final image analysis was done by a nuclear medicine physician. Separate analysis of the mammography and ultrasonographic images was executed by a radiologist and compared with the PET images in collaboration with the nuclear medicine physician to confirm that the tumor location on both imaging modalities was identical. Uptake of ^{89}Zr -bevacizumab in the tumor was quantified using AMIDE, A Medical Image Data Examiner software (version 0.9.3; Stanford University) (10). For the quantification of radioactivity within the tumor, 3-dimensional regions of interest were manually drawn around the tumor and axillary lymph node metastasis (if present). For determining the background also, uptake in the cardiac blood pool, normal breast (ipsi- and contralateral), and nipple was quantified. The data are presented as the maximum standardized uptake value (SUV_{max}). Furthermore, the images were analyzed for uptake of ^{89}Zr -bevacizumab along the cytology or biopsy channel.

Enzyme-Linked Immunosorbent Assay (ELISA) to Detect VEGF-A

For quantification of VEGF-A expression in the surgical specimen, ELISA was performed according to the manufacturer instructions (Quantikine; R&D Systems). Three random samples were collected from the surgical specimen of the primary tumor, ipsilateral normal tissue, and nipple tissue. Tissue was lysed manually using mammalian protein extraction reagent (M-PER; Pierce). Thereafter, mixtures were centrifuged at $20,000g$ for 15 min and subsequently stored at -20°C until analysis. Results of VEGF-A measurement were normalized for the protein concentration of the same samples determined by the Bradford assay (11).

Tumor Histology and Immunohistochemistry

Tumor tissue of the surgical specimen was typed and graded according to the World Health Organization guidelines and the modified Bloom and Richardson guidelines, respectively. Immunohistochemistry for VEGF-A and Ki-67 was performed on tumors, ductal carcinoma in situ (if present), and normal breast tissue using paraffin-embedded slides. Slides were deparaffinized in xylene and rehydrated in ethanol. Endogenous peroxidase was blocked by incubation with 0.3% hydrogen peroxidase for 30 min. The primary

antibodies rabbit anti-VEGF-A (A20-c152, 1:50; Santa Cruz Biotechnology), mouse anti-Ki-67 (1:300, clone MIB-1; DAKO), and mouse anti-CD31 (BD Pharmingen) were applied for 60 min, followed by suitable secondary antibodies, and immunostaining was visualized with 3'-diaminobenzidine tetrahydrochloride. Counterstaining was performed with hematoxylin. All stainings were scored by 2 independent observers. VEGF-A was scored (negative/positive) at $\times 400$ magnification. The proliferation index was calculated by counting of Ki-67-positive versus -negative cells in at least 5 high-power fields ($\times 400$). Microvessel density was scored in 5 areas defined as hot spots with the maximum number of microvessels.

Breast cancer molecular subtypes according to immunohistochemical profile were categorized as follows: luminal A (estrogen receptor [ER]-positive or progesterone receptor [PR]-positive and Ki-67 $< 14\%$), luminal B (ER-positive or PR-positive and Ki-67 $\geq 14\%$), human epidermal growth factor receptor 2 (HER2)-enriched (ER-negative, PR-negative, and HER2-positive), and basallike (ER-negative, PR-negative, HER2-negative). Luminal B also included tumors that were ER-positive or PR-positive and HER2-positive (12).

Phantom Study

To define the detection limit of the PET/CT camera system, a breast simulation phantom study was performed. Breast-shaped phantoms were produced as described earlier (13,14). For tumorlike agarose inclusions, 2% agarose (Hispanagar) was suspended in Tris-buffered saline and heated to 70°C . Subsequently, ^{89}Zr -oxalate was dissolved to a final concentration of 7,700 Bq/mL. Silicone molds were filled with the agarose mixture to create tumorlike inclusions ranging from 5 to 20 mm in diameter.

Breast phantoms were constructed with 2 tumorlike inclusions. PET imaging was performed on day 1 and every 3–4 d until visual disappearance of the lesions from the scan. Final image analysis was performed as stated above. The recovery coefficient was determined by calculating the ratio between the measured amount of ^{89}Zr on the PET image and the inserted dose as measured by a dose calibrator, corrected for decay.

Statistical Analyses

Data are presented as a mean \pm SD. Statistical analysis was performed using the paired *t* test or Wilcoxon signed rank test for paired data and the unpaired *t* test for unpaired data. Associations between parameters were evaluated using the Pearson correlation test (SPSS, version 19.0; IBM). A double-sided *P* value of less than 0.05 was considered significant.

RESULTS

Patient Characteristics

A total of 23 patients with 26 breast tumors was included. The patients had no history of prior malignancies. Two women had bilateral breast cancer, and 1 patient had 2 ipsilateral tumors. Patient and tumor characteristics are shown in Table 1. Breast tumors were detected with mammography ($n = 22$), ultrasound ($n = 25$), or MR imaging ($n = 1$). Histologic analyses showed invasive ductal carcinoma ($n = 23$), invasive lobular carcinoma ($n = 2$), and invasive tubular carcinoma ($n = 1$). Of the 25 available invasive cancers, 9 tumors were classified as luminal A breast cancer and 14 as luminal B. There was 1 basallike and 1 HER2-enriched tumor. Six patients had pathologically proven axillary lymph node metastases before surgery. In 3 additional patients, tumor cells were detected in the sentinel lymph node after surgery. In a patient with bilateral breast cancer, axillary lymph node involvement on one side was already known before surgery and was also detected in a sentinel lymph node of the opposite axilla.

TABLE 1
Patient and Tumor Characteristics

Characteristic	Data
Tumors (n)	26
Patients (n)	23
Age of patients (y)	
Median \pm SD	54.9 \pm 10.2
Range	32–73
Tumor size (mm)	
Median \pm SD	25.1 \pm 19.8
Range	4–80
Tumor type (n)	
Invasive ductal carcinoma	23
Invasive lobular carcinoma	2
Invasive tubular carcinoma	1
Tumor stage (n)	
T1	15
T2	5
T3	5
T4	1
Nodal stage (n)	
N0	15
N1	4
N2	2
N3	4

⁸⁹Zr-Bevacizumab PET

In this study, no adverse events were seen. ⁸⁹Zr-bevacizumab PET imaging showed uptake in 25 of the 26 breast tumors (96.1%). Figure 1 shows a representative example. Uptake of ⁸⁹Zr-bevacizumab was higher in breast tumors than in normal breast tissue (of both the ipsi- and contralateral breast); SUV_{max} was 1.85 ± 1.22 (range, 0.52–5.64) in breast tumors versus 0.59 ± 0.37 (range, 0.27–1.69) in ipsilateral normal breast tissue and 0.51 ± 0.26 (range, 0.20–1.12) in contralateral normal breast tissue (both $P < 0.001$) (Fig. 2A). There was similar ⁸⁹Zr-bevacizumab uptake in normal tissue of both breasts ($P = 0.88$). The SUV_{max} of luminal A tumors was 1.28 ± 0.58 , compared with 2.04 ± 1.08 in luminal B tumors ($P = 0.06$). In the patients with a basallike and HER2-overexpressing breast tumor, SUV_{max} was 0.52 and 5.64, respectively. The only breast tumor that did not show preferential ⁸⁹Zr-bevacizumab uptake was an invasive ductal carcinoma with a diameter of 10 mm. Lymph node metastases (size range, 3–42 mm) were present in 10 axillary regions (of 9 patients); 4 of these lymph node–positive axillary regions were detected by PET (SUV_{max}, 2.66 ± 2.03 ; range, 1.32–5.68). On the basis of ultrasound and cytology, all 4 positive axillary regions were already known before

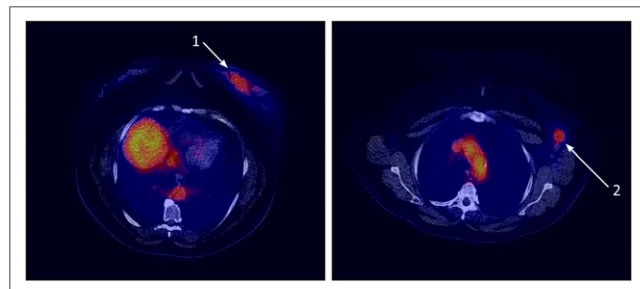


FIGURE 1. Axial slices of ⁸⁹Zr-bevacizumab PET from patient with primary breast tumor (1) and lymph node metastasis (2).

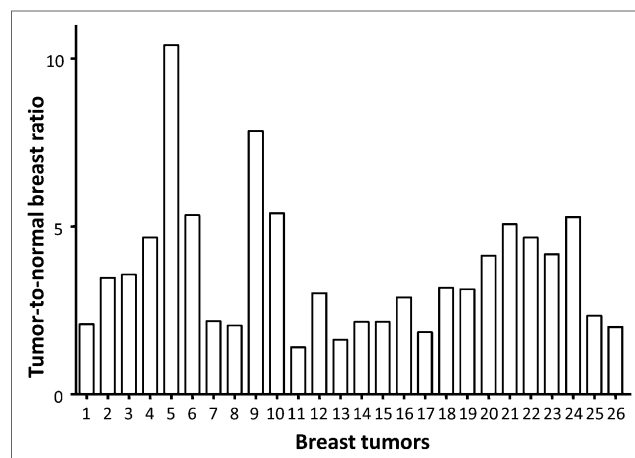


FIGURE 2. Analysis per patient (x-axis) showing ratio between ⁸⁹Zr-bevacizumab uptake expressed as SUV_{max} in breast tumors vs. normal breast tissue.

surgery. ⁸⁹Zr-bevacizumab PET detected none of 4 positive axillary regions with 1–3 lymph node metastases (pN1) and 4 of 6 positive axillary regions with 4 or more lymph node metastases (\geq pN2). There were no false-positive readings, and there was no ⁸⁹Zr-bevacizumab uptake along the cytology or biopsy tract.

Next to tumor visualization, there was slightly higher uptake in the nipples of both breasts than in the background in 20 of the 23 patients. The SUV_{max} of nipple tissue was 1.13 ± 0.59 (range, 0.47–3.02). This is lower than the SUV_{max} in tumor tissue ($P = 0.01$). The SUV_{max} in the blood pool on day 4 was 4.17 ± 1.07 (range, 2.97–7.05), which is 2.3- and 3.7-fold higher than in the tumors and nipples, respectively.

VEGF-A ELISA

For VEGF-A ELISA measurements, surgical specimens of 17 breast tumors and 24 specimens of normal ipsilateral breast tissue were available. Pathologic examination of the tissue confirmed tumor in all macroscopic tumors. Mean tumor VEGF-A/mg of protein was higher (184 ± 169 pg) than in normal breast tissue (10 ± 21 pg, $P = 0.001$) (Fig. 2B). In the 10-mm tumor that was not detected by ⁸⁹Zr-bevacizumab PET, 371 pg of VEGF-A per milligram of protein was measured. ⁸⁹Zr-bevacizumab tumor uptake of the ⁸⁹Zr-bevacizumab–detected tumors correlated with the VEGF-A protein level (Pearson $r = 0.49$, $P = 0.04$) (Fig. 3).

In the 11 available nipple specimens (including both nipples from 1 patient with bilateral breast cancer), the VEGF-A level was 10 ± 13 pg per milligram of protein, which was not different from normal breast tissue ($P = 0.96$).

Immunohistochemistry

All available tumors ($n = 25$) showed positive staining for VEGF-A expression. VEGF-A expression in normal tissue was absent in 2 and present in 23 of the 25 operated breasts. Ductal carcinoma in situ was present in 10 patients and stained positively for VEGF-A in all cases. ⁸⁹Zr-bevacizumab tumor uptake correlated positively with a mean proliferation index of 32.1 ± 24.3 (range, 6.0–86.0) (Pearson $r = 0.55$, $P = 0.005$) (Fig. 4). The microvessel density did not correlate with ⁸⁹Zr-bevacizumab uptake ($r = 0.10$, $P = 0.64$).

Phantom Study

All tumorlike inclusions were visible on day 1. The recovery coefficient was 73% for the smallest inclusion and 96% for the

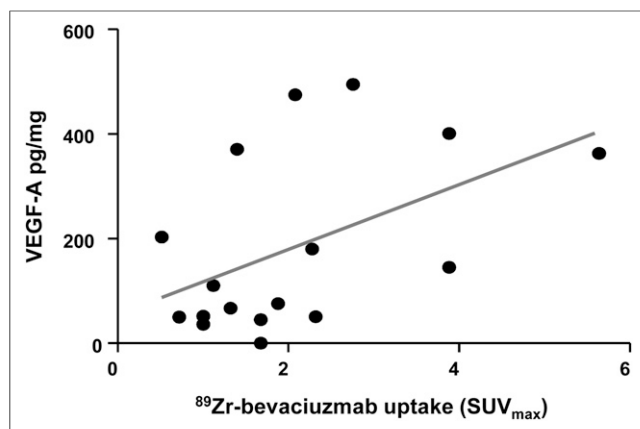


FIGURE 3. Correlation between ^{89}Zr -bevacizumab tumor uptake (x-axis) and tumor VEGF-A (y-axis) levels as measured by ELISA (Pearson $r = 0.49$, $P = 0.04$).

largest one. The last time point before visual disappearance was day 1 (5-mm inclusion), day 10 (10-mm inclusion), day 14 (15-mm inclusion), and day 17 (20-mm inclusion).

DISCUSSION

To our knowledge, this was the first clinical feasibility study with ^{89}Zr -bevacizumab PET in breast cancer patients. Uptake of ^{89}Zr -bevacizumab was visualized in 96.1% of the primary tumor lesions, and there was a relation with the level of VEGF-A in the tumor. This result provides proof that ^{89}Zr -bevacizumab might be potentially valuable for biologic characterization of tumors and for prediction and evaluation of the effect of VEGF-A–targeting therapeutics.

VEGF-A is reported in several studies to be overexpressed in malignant breast tumors and in ductal carcinoma in situ (5,15), thus covering the full spectrum from early-stage breast cancer to more advanced stages. More frequent VEGF-A staining was found to be related to aggressiveness as assessed by VEGF-A staining in a study with 1,788 breast tumors (5). ^{89}Zr -bevacizumab PET proved to be able to detect a broad range of VEGF-A expression levels. Quantitative tumor analyses showed a more than 10-fold

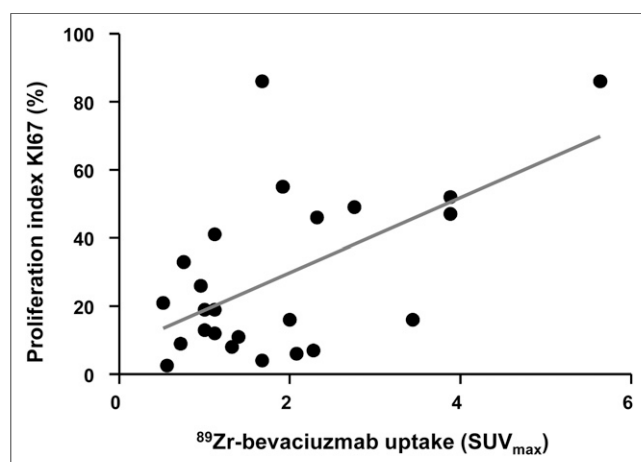


FIGURE 4. Correlation between ^{89}Zr -bevacizumab tumor uptake (x-axis) and proliferation index (y-axis) as measured with Ki-67 expression by tumor (Pearson $r = 0.55$, $P = 0.005$).

difference between individual SUV_{max} measurements, suggesting large differences in VEGF-A tumor levels between patients, as was confirmed by the broad difference in VEGF-A measured by ELISA. Although there was a high visualization rate, the SUV_{max} of tumors and normal tissues did overlap in this study. Importantly, in individual patients SUV_{max} was always higher in tumor than in normal breast tissues. The higher VEGF-A ratio between tumor and normal breast as measured by ELISA than by PET might be explained by the fact that (in contrast to ^{89}Zr -bevacizumab PET) ELISA also measures intracellular VEGF-A (16). Moreover, the resolution of the PET camera is 10 mm whereas ELISA and immunohistochemistry measure on the cellular level.

^{89}Zr -bevacizumab uptake in the primary breast tumors was relatively low, compared with uptake in a series of 22 metastatic renal cell cancers in our institution (mean SUV_{max} , 1.85 vs. 10.1) (15). Antiangiogenic treatment has monotherapy activity in renal cell cancers but not in tumor types such as breast cancer (17,18). The difference in ^{89}Zr -bevacizumab uptake, and therefore VEGF-A levels, is possibly related to this varying efficacy. ^{89}Zr -bevacizumab might be potentially valuable for biologic characterization of tumors and for prediction and evaluation of the effect of VEGF-A–targeting therapeutics.

The failure to detect the tumor lesion 10 mm in diameter despite sufficient VEGF-A expression can be explained by the findings in our phantom study. Small lesions visually disappear much earlier on ^{89}Zr -PET than do larger lesions. This effect might influence tumor uptake of ^{89}Zr -bevacizumab measured by SUV_{max} . The observed effect of tumor size on PET detection is shared by ^{18}F -FDG PET (19,20) but is larger in the case of ^{89}Zr -PET. Because of the higher radiation dose per megabecquerel of ^{89}Zr , a lower amount of activity was injected for ^{89}Zr than for ^{18}F -FDG. ^{89}Zr has a smaller yield of positrons than does ^{18}F , resulting in increased noise, and therefore ^{89}Zr -bevacizumab PET images require more smoothing. This degrades resolution and increases size effects. Importantly, imaging with ^{89}Zr -bevacizumab PET delivered no false-positive lesions.

Most patients had uptake of ^{89}Zr -bevacizumab in the region of the nipple, whereas the VEGF-A level as measured with ELISA was low and equal to that in normal tissue. ^{89}Zr has a long half-life of 78.4 h. When labeled to bevacizumab, a considerable amount of the tracer remains in the circulation. Therefore, uptake of ^{89}Zr -bevacizumab in the nipple is likely to be due to high vascularization of the nipple, compared with normal breast tissue (21). In the tumor, the contribution of perfusion to increased ^{89}Zr -bevacizumab uptake in the tumor is less likely to play a role, based on preclinical and clinical data. In a xenograft mouse model, we have shown that tumor accumulation of ^{89}Zr -bevacizumab increases in time, whereas uptake in normal organs decreases (6). This increase in ^{89}Zr -bevacizumab tumor accumulation over time was also shown in melanoma patients who underwent ^{111}In -bevacizumab SPECT (9). In a human SKOV-3 ovarian tumor xenograft, there was higher uptake of ^{89}Zr -bevacizumab than of ^{89}Zr -IgG (6), indicating tumor-specific uptake. ^{89}Zr -IgG PET in the patient setting is not possible because of radiation exposure concerns. This is also the limiting factor in using ^{89}Zr -bevacizumab PET in healthy subjects as a negative control. However, the microvessel density did not influence ^{89}Zr -bevacizumab uptake. Moreover, the relation between VEGF-A measured by ELISA and ^{89}Zr -bevacizumab uptake in tumors and not in nipple tissue is in line with the preclinical finding that the tracer uptake is, in fact, tumor-specific.

The limiting factor for more general application of imaging with radionuclides is the radiation burden. In a study comparing the risks of radiation-induced cancer from mammography, molecular breast imaging, and positron emitting mammography, the cumulative cancer incidence is 15–30 times higher for positron emission mammography and molecular breast imaging than for mammography (22). The estimated radiation burden of ^{89}Zr -bevacizumab-PET is 19 mSv per tracer injection, on the basis of extrapolation from ^{111}In -bevacizumab data and a dosimetry study on ^{89}Zr -U36, compared with 5.3 mSv for ^{18}F -FDG PET (23–25).

To make optimal use of the tumor specificity of molecular imaging of VEGF-A while overcoming radiation issues, bevacizumab was also linked to the near-infrared fluorescent dye IRDye 800CW in our institution. This technique has already been tested in human xenograft-bearing athymic mice, detecting tumor lesions in vivo with high sensitivity and specificity. IRDye 800CW-labeled bevacizumab revealed submillimeter lesions with a clinical intraoperative fluorescence camera (26). Recently, we started a study with IRDye 800CW-labeled bevacizumab in early breast cancer (NCT01508572). The aim of this study is to determine the uptake of the VEGF-A-targeting fluorescent tracer in breast tumors, both during preoperative diffuse optical tomography and during surgery. This approach can potentially contribute to the development of a tumor-specific tracer.

CONCLUSION

In this first clinical feasibility study with ^{89}Zr -bevacizumab PET in breast cancer patients, we have shown that uptake of ^{89}Zr -bevacizumab was visible in most primary breast tumors and correlated with the protein level of VEGF-A in the tumor. These findings support use of VEGF-A imaging in breast cancer for future imaging purposes.

DISCLOSURE

The costs of publication of this article were defrayed in part by the payment of page charges. Therefore, and solely to indicate this fact, this article is hereby marked “advertisement” in accordance with 18 USC section 1734. This work was supported by the Dutch Cancer Society (grant RUG 2009-4273), the Dutch Pink Ribbon Foundation, and the foundation A Sister’s Hope (grant KP566481). No other potential conflict of interest relevant to this article was reported.

ACKNOWLEDGMENTS

We thank Arieke Prozée, Kees Meijer, and Marian Beernink for their assistance with patient inclusion in the trial and Tineke van der Sluis and Esther M.E. van Straten for their technical assistance.

REFERENCES

1. Ferlay J, Shin HR, Bray F, Forman D, Mathers C, Parkin DM. Estimates of worldwide burden of cancer in 2008: GLOBOCAN 2008. *Int J Cancer*. 2010;127:2893–2917.
2. Vogl G, Bartel H, Dietze O, Hauser-Kronberger C. HER2 is unlikely to be involved in directly regulating angiogenesis in human breast cancer. *Appl Immunohistochem Mol Morphol*. 2006;14:138–145.
3. Kostopoulos I, Arapantoni-Dadioti P, Gogas H, et al. Evaluation of the prognostic value of HER-2 and VEGF in breast cancer patients participating in a randomized study with dose-dense sequential adjuvant chemotherapy. *Breast Cancer Res Treat*. 2006;96:251–261.
4. Fuckar D, Dekanic A, Stifter S, et al. VEGF expression is associated with negative estrogen receptor status in patients with breast cancer. *Int J Surg Pathol*. 2006;14:49–55.
5. Liu Y, Tamimi RM, Collins LC, et al. The association between vascular endothelial growth factor expression in invasive breast cancer and survival varies with intrinsic subtypes and use of adjuvant systemic therapy: results from the Nurses’ Health Study. *Breast Cancer Res Treat*. 2011;129:175–184.
6. Nagengast WB, de Vries EG, Hospers GA, et al. In vivo VEGF imaging with radiolabeled bevacizumab in a human ovarian tumor xenograft. *J Nucl Med*. 2007;48:1313–1319.
7. Nagengast WB, de Korte MA, Oude Munnink TH, et al. ^{89}Zr -bevacizumab PET of early antiangiogenic tumor response to treatment with HSP90 inhibitor NVP-AUY922. *J Nucl Med*. 2010;51:761–767.
8. Oosting SF, Brouwers AH, Van Es SC, et al. ^{89}Zr -bevacizumab PET imaging in metastatic renal cell carcinoma patients before and during antiangiogenic treatment. *J Clin Oncol*. 2012;30(suppl): abstract 10581.
9. Nagengast WB, Hooge MN, van Straten EM, et al. VEGF-SPECT with ^{111}In -bevacizumab in stage III/IV melanoma patients. *Eur J Cancer*. 2011;47:1595–1602.
10. Loening AM, Gambhir SS. AMIDE: a free software tool for multimodality medical image analysis. *Mol Imaging*. 2003;2:131–137.
11. Bradford MM. A rapid and sensitive method for the quantitation of microgram quantities of protein utilizing the principle of protein-dye binding. *Anal Biochem*. 1976;72:248–254.
12. Goldhirsch A, Wood WC, Coates AS, et al. Strategies for subtypes: dealing with the diversity of breast cancer—highlights of the St. Gallen International Expert Consensus on the Primary Therapy of Early Breast Cancer 2011. *Ann Oncol*. 2011;22:1736–1747.
13. De Grand AM, Lomnes SJ, Lee DS, et al. Tissue-like phantoms for near-infrared fluorescence imaging system assessment and the training of surgeons. *J Biomed Opt*. 2006;11:014007.
14. Pleijhuis RG, Langhout GC, Helfrich W, et al. Near-infrared fluorescence (NIRF) imaging in breast-conserving surgery: assessing intraoperative techniques in tissue-simulating breast phantoms. *Eur J Surg Oncol*. 2011;37:32–39.
15. Bluff JE, Menakuru SR, Cross SS, et al. Angiogenesis is associated with the onset of hyperplasia in human ductal breast disease. *Br J Cancer*. 2009;101:666–672.
16. Toi M, Kondo S, Suzuki H, et al. Quantitative analysis of vascular endothelial growth factor in primary breast cancer. *Cancer*. 1996;77:1101–1106.
17. Brufsky AM, Hurvitz S, Perez E, et al. RIBBON-2: a randomized, double-blind, placebo-controlled, phase III trial evaluating the efficacy and safety of bevacizumab in combination with chemotherapy for second-line treatment of human epidermal growth factor receptor 2-negative metastatic breast cancer. *J Clin Oncol*. 2011;29:4286–4293.
18. Yang JC, Haworth L, Sherry RM, et al. A randomized trial of bevacizumab, an anti-vascular endothelial growth factor antibody, for metastatic renal cancer. *N Engl J Med*. 2003;349:427–434.
19. Avril N, Rose CA, Schelling M, et al. Breast imaging with positron emission tomography and fluorine-18 fluorodeoxyglucose: use and limitations. *J Clin Oncol*. 2000;18:3495–3502.
20. Veronesi U, De Cicco C, Galimberti VE, et al. A comparative study on the value of FDG-PET and sentinel node biopsy to identify occult axillary metastases. *Ann Oncol*. 2007;18:473–478.
21. O’Dey D, Prescher A, Pallua N. Vascular reliability of nipple-areola complex-bearing pedicles: an anatomical microdissection study. *Plast Reconstr Surg*. 2007;119:1167–1177.
22. O’Connor MK, Li H, Rhodes DJ, Hruska CB, Clancy CB, Vetter RJ. Comparison of radiation exposure and associated radiation-induced cancer risks from mammography and molecular imaging of the breast. *Med Phys*. 2010;37:6187–6198.
23. de Jong JR, Warnders FJ, Nagengast WB, et al. Radiation dosimetry of ^{111}In -bevacizumab for VEGF-SPECT in melanoma patients. *Eur J Nucl Med Mol Imaging*. 2010;37(suppl):S477–S477.
24. Börjesson PK, Jauw YW, de Bree R, et al. Radiation dosimetry of ^{89}Zr -labeled chimeric monoclonal antibody U36 as used for immuno-PET in head and neck cancer patients. *J Nucl Med*. 2009;50:1828–1836.
25. Murano T, Minamimoto R, Senda M, et al. Radiation exposure and risk-benefit analysis in cancer screening using FDG-PET: results of a Japanese nationwide survey. *Ann Nucl Med*. 2011;25:657–666.
26. Terwisscha van Scheltinga AG, van Dam GM, Nagengast WB, et al. Intraoperative near-infrared fluorescence tumor imaging with vascular endothelial growth factor and human epidermal growth factor receptor 2 targeting antibodies. *J Nucl Med*. 2011;52:1778–1785.



The Journal of
NUCLEAR MEDICINE

^{89}Zr -Bevacizumab PET Imaging in Primary Breast Cancer

Sietske B.M. Gaykema, Adrienne H. Brouwers, Marjolijn N. Lub-de Hooge, Rick G. Pleijhuis, Hetty Timmer-Bosscha, Linda Pot, Gooitzen M. van Dam, Sibylle B. van der Meulen, Johan R. de Jong, Joost Bart, Jakob de Vries, Liesbeth Jansen, Elisabeth G.E. de Vries and Carolien P. Schröder

J Nucl Med. 2013;54:1014-1018.

Published online: May 7, 2013.

Doi: 10.2967/jnumed.112.117218

This article and updated information are available at:

<http://jnm.snmjournals.org/content/54/7/1014>

Information about reproducing figures, tables, or other portions of this article can be found online at:

<http://jnm.snmjournals.org/site/misc/permission.xhtml>

Information about subscriptions to JNM can be found at:

<http://jnm.snmjournals.org/site/subscriptions/online.xhtml>

The Journal of Nuclear Medicine is published monthly.
SNMMI | Society of Nuclear Medicine and Molecular Imaging
1850 Samuel Morse Drive, Reston, VA 20190.
(Print ISSN: 0161-5505, Online ISSN: 2159-662X)

© Copyright 2013 SNMMI; all rights reserved.

 SOCIETY OF
NUCLEAR MEDICINE
AND MOLECULAR IMAGING